

# Technical note: „U-Th Analysis” – an open-source software dedicated to MCICPMS U-series-data treatment and evaluation

Inga Kristina Kerber<sup>1</sup>, Fabian Kontor<sup>1</sup>, [Aaron Mielke<sup>1,2</sup>](#), Sophie Warken<sup>1,2</sup>, Norbert Frank<sup>1\*</sup>

<sup>1</sup> Institute for Environmental Physics, Heidelberg University, Heidelberg, Germany

<sup>2</sup> Institute for Earth Sciences, Heidelberg University, Heidelberg, Germany

Correspondence to: Norbert Frank (<mailto:norbert.frank@iup.uni-heidelberg.de>)

Feldfunktion geändert

## Abstract

We present our standalone data analysis application for  $^{230}\text{Th}/\text{U}$  dating on multi-collector inductively coupled plasma mass spectrometers (MC-ICP-MS). The Python-based algorithm is equipped with a graphical user interface (GUI) and comprises raw data treatment, corrections, age calculation, and error estimation. Our underlying measurement protocol employs a combination of Faraday cups (FC) and secondary electron multipliers (SEM), and the software allows for different detector layouts for the measurement of the least abundant isotopes  $^{234}\text{U}$ ,  $^{230}\text{Th}$  and  $^{229}\text{Th}$ . We especially focus on features that ensure reproducibility and enable user-friendly reanalysis of measurements such as customized calculation constants with templates. Result files are saved automatically and contain all relevant settings used. Eventually, we demonstrate the relevance of adequate data outlier treatment and generally recommend using the median instead of the mean of calculated ratios. The performance of our evaluation software is demonstrated by a case study from a Puerto Rican stalagmite with growth phases from modern to 40 ka old. The majority of the obtained ages reaches uncertainties in the range of 0.3-0.6%, underlining the capability of our measurement protocol.

## 1 Introduction

The U-series disequilibrium method,  $^{230}\text{Th}/\text{U}$  dating, is a precise chronometer covering approximately the last 650 kiloyears, and has proven indispensable for the age determination of marine and continental carbonate archives and their applications (Bourdon et al., 2003). The method is based on a complete disequilibrium of  $^{234}\text{U}$ , with its daughter nuclide  $^{230}\text{Th}$ , during the formation of secondary carbonates. It presumes a subsequent closed system evolution of the activity ratio of ( $^{230}\text{Th}/^{234}\text{U}$ ) and ( $^{234}\text{U}/^{238}\text{U}$ ) since the time of formation. Ideally, the initial  $^{230}\text{Th}$  activity of the material is presumed zero or can be estimated from the total Th concentration via an initial ( $^{230}\text{Th}/^{232}\text{Th}$ ) activity ratio. The dating applications for secondary carbonates and other appropriate materials are manifold in geochemistry, archaeology, and climate science. ~~The applications relying on this dating method are manifold in geochemistry, archaeology and climate science.~~ Further development of this dating method includes both improvements in instrumentation and measurement protocols, as well as reproducible data analysis and age calculation schemes (Pourmand et al., 2014; Andersen et al., 2004; Cheng et al., 2013; Breton et al., 2015; Chiang et al., 2019; Hellstrom, 2003; Hoffmann et al., 2007; Shen et al., 2002; Shen et al., 2012; Kerber et al., 2023; Shao et al., 2019). The presently most sensitive and precise technology for high precision U and Th isotope

37 measurements is multi-collector inductively coupled plasma source mass spectrometry (MC-ICPMS). Recent  
38 technological advances of MC-ICP-MS include the implementation of high ohmic amplifiers allowing to enhance  
39 the dynamic range of multiple Faraday-collectors (FC) to six orders of magnitude for the simultaneous detection  
40 of very large and low isotope abundances, instead of the conventionally used combination of secondary electron  
41 multipliers (SEM) and FC (Breton et al., 2015). Measurement protocol updates aim at increasing measurement  
42 precision and/or decreasing input sample masses by combining new detector layouts, improving the understanding  
43 of correction factors, and ensuring a stable measurement environment (Cheng et al., 2013; Chiang et al., 2019;  
44 Shen et al., 2002; Shen et al., 2012; Hellstrom, 2003; Andersen et al., 2004; Hoffmann et al., 2007; Kerber et al.,  
45 2023; Shao et al., 2019).

46 We here focus on the third route for the enhancement of  $^{230}\text{Th}/\text{U}$  dating, which is clear and reproducible data  
47 analysis and age calculation schemes. Up to now, only two  $^{230}\text{Th}/\text{U}$  dating data analysis routines have been  
48 published (Shao et al., 2019; Pourmand et al., 2014). However, regarding the rising amount of data being produced  
49 in MC-ICP-MS laboratories, data management is becoming more and more important. For example, some samples  
50 might require later adaptation of the individual corrections of isotope ratios due to residual contamination with  
51 non-carbonate material or detection of initial  $^{230}\text{Th}$  from the carbonate forming environment.

52 Dating young materials of only a few years to centuries in age is challenging  $\oplus$  due to the small number of counts  
53 on especially  $^{230}\text{Th}$ , which implies that all correction factors including “ghost signal” corrections need to be  
54 determined very precisely (Zhao et al., 2009; Chiang et al., 2019; Kerber et al., 2023). Regarding the removal of  
55 scatter ions on the specific low abundance masses 230 and 229 amu, Kerber et al. (2023) demonstrated an effective  
56 correction based on a linear dependence of the scattered ions on the  $^{238}\text{U}$  signal. Other authors separate U and Th  
57 chemically to reduce or remove the  $^{238}\text{U}$  beam from the low abundance Thorium isotope measurements (Chiang  
58 et al., 2019), which implies flexibility in the detector arrangement and data treatment protocol. As such scatter  
59 peaks may depend on the specific instrument or vary through time, these corrections need to be adaptable constants  
60 in the data evaluation routine. The influence on final atomic ratio and accuracy of the ghost signals as well as by  
61 typical variation in other individual corrections such as peak tailing, mass fractionation, isobaric interferences are  
62 evaluated in detail in Kerber et al. (2023).

63 In addition, the correction for initial Thorium may cause large age corrections and propagated uncertainties, in  
64 particular since adequate initial Th values based on the  $^{230}\text{Th}/^{232}\text{Th}$  ratio may be variable and difficult to detect  
65 (Hellstrom, 2006; Wenz et al., 2016; Wortham et al., 2022). There are different methods to estimate the initial Th  
66 isotope ratio: First, isochrons can be used to determine the isotopic composition of the detrital component in the  
67 carbonate (Ludwig and Titterton, 1994; Wenz et al., 2016; Stinnesbeck et al., 2020; Töchterle et al., 2022).  
68 Secondly, analyses of modern drip waters or recent carbonate deposits allow estimation of the value and sources  
69 of initial Th (Wortham et al., 2022; Li et al., 2022). In some cases the “true” age of a stalagmite can be also  
70 inferred from other dating methods, such as radiocarbon (Akers et al., 2019; Huang et al., 2024) or the  
71 stratigraphic order (Hellstrom, 2006). Also, several approaches can be combined (Warken et al., 2020; Akers et  
72 al., 2016; Roy-Barman and Pons-Branchu, 2016).

73 Other aspects are updating half-lives (such as e. g. from Cheng et al. (2000b) to Cheng et al. (2013)), which makes  
74 re-evaluation of previously measured data necessary. These tasks are error-prone, in particular when they require  
75 copy-and-pasting data in e. g. spreadsheets. Also, a clear and unified documentation of the applied constants and  
76 the way of saving data is desirable. Additionally, the statistical methods, for example for outlier correction, should

77 undergo clear documentation. Altogether, this helps to report Th/U ages in a standardized way (Dutton et al.,  
78 2017).

79 In this study, we present our user-friendly GUI and the underlying algorithm for data treatment and age  
80 calculation. The software is currently optimized for ThermoFisher Neptune MC-ICP-MS instruments, but the  
81 open-source code in principle allows adaptations to other setups and instruments. Methods to treat outliers in  
82 measurement data are particularly highlighted. As a case study, we present newly obtained ages from a stalagmite  
83 from Larga Cave, Puerto Rico, which shows a modern growth phase, as well as continuous deposition during the  
84 last Glacial into the deglaciation, thus demonstrating the performance of our method for both very young and  
85 older sample materials. Our protocol enables a precise determination of speleothem growth rates, which allows a  
86 comparison to a coevally deposited stalagmite from the same cave highlighting the influence of in-cave processes  
87 on speleothem growth rates. In particular, this dataset showcases how initial  $^{230}\text{Th}$  correction models can be easily  
88 tested with our here presented software and GUI, and how those influence speleothem chronologies.

## 89 2 Methods

### 90 2.1 Standards and reference materials

91 We use our in-house triple spike solution (TriSpike) with a  $^{233}\text{U}$  concentration of  $(0.038556 \pm 0.0000009)$  ng/g, a  
92  $^{236}\text{U}$  concentration of  $(3.86778 \pm 0.00009)$  ng/g and a  $^{229}\text{Th}$  concentration of  $(0.018055 \pm 0.000008)$  ng/g (2  
93 standard error of the mean) (Kerber et al., 2023). For standard bracketing, we employ the Harwell-Uraninite 1  
94 (HU-1) as a reference material. Its activity ratios ( $^{230}\text{Th}/^{238}\text{U}$ ) and ( $^{234}\text{U}/^{238}\text{U}$ ) are presumed to be 1, as it is a secular  
95 equilibrium material. Abundance sensitivity and hydride correction are determined by measuring CRM-112A U  
96 reference solution and an in-house  $^{232}\text{Th}$  standard. The CRM-112A gravimetric standard solution has a  $^{238}\text{U}$   
97 concentration of  $(4.3021 \pm 0.0015)$   $\mu\text{g/g}$ , while the inhouse  $^{232}\text{Th}$  standard calibrated with TriSpike has a  $^{232}\text{Th}$   
98 concentration of  $(505.8 \pm 1.02)$  ng/g (2  $\sigma$  uncertainties). CRM-112A solution is also used to track the values of  
99 the two ghost signal constants,  $k_{229}$  and  $k_{230}$  (Kerber et al., 2023). For  $k_{229}$ , it is measured without addition of  
100 TriSpike, while in the case of  $k_{230}$ , the spiked CRM-112A solution is employed. For age determination, the  $^{230}\text{Th}$   
101 and  $^{234}\text{U}$  decay constants determined by Cheng et al. (2013) are used. Ages are reported with 2  $\sigma$  statistical standard  
102 mean error, but -do not include half-life uncertainties.

### 103 2.2 Chemical preparation and instrumentation

104 The chemical preparation of carbonate samples includes sample dissolution in ultra clean nitric acid, spiking with  
105 TriSpike and two steps of wet column chromatographic ion exchange separation of U and Th from matrix elements  
106 using Eichrom UTEVA resin (Douville et al., 2010; Wefing et al., 2017; Matos et al., 2015). Chemical blanks are  
107 commonly below 0.4 fg for  $^{234}\text{U}$  and 0.04 fg for  $^{230}\text{Th}$  and Ca matrix concentrations are required to be below 10  
108 ppm. For the mass-spectrometric measurement, samples are dissolved in 1 %  $\text{HNO}_3$  and 0.05 % HF. All samples  
109 were measured on a MC-ICP-MS (ThermoFisher Neptune Plus) at the Institute for Environmental Physics,  
110 Heidelberg University (Germany). The desolvating system CETAC Aridus II is used as inlet.  
111 The mass spectrometer is equipped with Faraday cups (FC) and a central secondary electron multiplier (SEM).  
112 The central detector can be selected between the SEM and a FC connected to a  $10^{13} \Omega$  amplifier.  $^{238}\text{U}$  is measured  
113 on a  $10^{10} \Omega$  amplified resistor. All other FC are connected to  $10^{11} \Omega$  amplifiers. The cup setting to collect isotope  
114 signals on masses 238 to 229 follows the one shown in table 2 in table 2 in Kerber et al. (2023). The first cycle collects all U isotopes for



154 Larga Cave is located in the north central karst region of Puerto Rico (supplementary Figure S1A). Previous work  
155 including extensive cave air and drip monitoring has demonstrated that the cave is a valuable location to study of  
156 the influence of changing climate on past rainfall patterns in the Western tropical Atlantic (Vieten et al., 2018a;  
157 Warken et al., 2022b; Vieten et al., 2018b). In particular, the main passage of Larga Cave is subject to a seasonally  
158 varying ventilation, which results in pCO<sub>2</sub> values of 600 ppm close to atmospheric values during winter, and  
159 higher values up to 1800 ppm in summer (Vieten et al., 2016). In contrast, in the deep part of the cave, where also  
160 stalagmite B1 was collected, ventilation is strongly muted, and cave air pCO<sub>2</sub> values are higher with values up to  
161 2300 – 3600 ppm (Vieten et al., 2016). As a result of this ventilation regime, growth rates are expected to vary  
162 both seasonally, but also between different locations inside the cave (Vieten and Hernandez, 2021).

### 163 3 Data treatment and analysis procedures

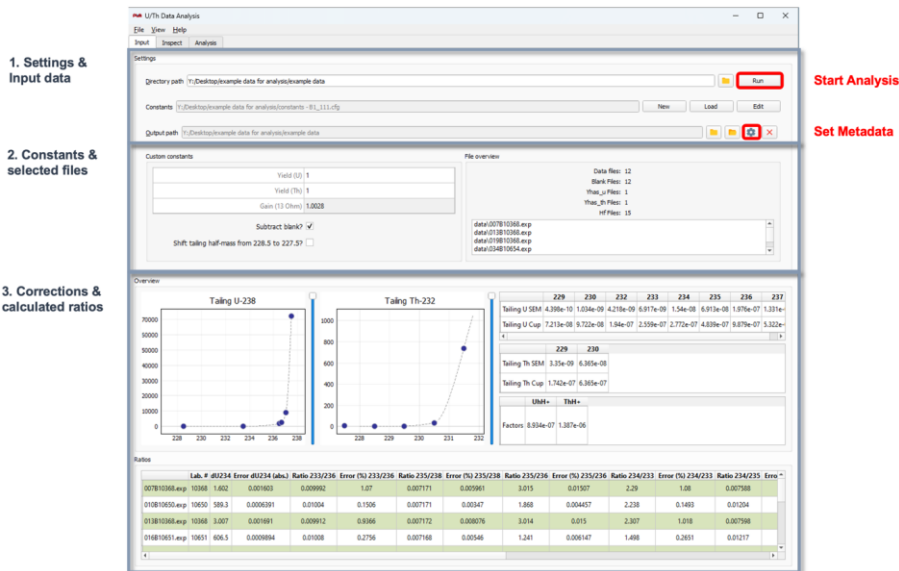
164 The whole analysis procedure from raw data treatment to age calculation is conducted in one GUI featuring three  
165 tabs: ‘Input’ for isotopic ratio calculations, ‘Inspect’ for outlier correction of the signal and ‘Analysis’ for age  
166 calculation. The source code is accessible at [https://github.com/puad/UTh\\_Analysis](https://github.com/puad/UTh_Analysis) ~~[https://github.com/Enw/Archived-UTh\\_Analysis](https://github.com/Enw/Archived-UTh_Analysis)~~. It is based on the open  
167 source PyQt5 Python library (<https://pypi.org/project/PyQt5/>). To execute the GUI, the user has to run the file  
168 `main.py`. The folder [https://github.com/puad/UTh\\_Analysis/tree/main](https://github.com/puad/UTh_Analysis/tree/main) ~~[https://github.com/Enw/Archived-UTh\\_Analysis/tree/main](https://github.com/Enw/Archived-UTh_Analysis/tree/main)~~ contains the complete code for the GUI  
169 (“UTh Data Analysis.exe”) as well as default configuration files (“constants – coral.cfg” and “constants –  
170 stalag.cfg”). Input and output format of files are .csv or .xlsx. The GUI consists of three consecutive tabs, for which  
171 the functionalities and the underlying calculations and processes will be described in the following.

Feldfunktion geändert

#### 172 3.1 Input tab

173 In ‘Input’, as presented in [Figure 1](#) ~~[Figure 4](#)~~, the user can navigate to the folder containing the raw mass spectrometer data  
174 and start the calculation of corrected isotopic ratios (Box 1 in [Figure 1](#) ~~[Figure 4](#)~~). All tab screenshots present data from  
175 stalagmite B1. Prior to the calculations, a configuration file containing all necessary constants used in the  
176 calculations needs to be loaded (same Box 1). This file contains constants and correction factors used for  
177 evaluation of the activity ratios and ages, such as mass fractionation coefficients, decay constants, the exact masses  
178 of the isotopes and the values applied for initial <sup>230</sup>Th correction model. All constants can be edited manually  
179 either in the configuration file directly, or within the GUI using the button “edit”. An exemplary configuration  
180 table is also provided in the supplementary material (Figure S2). To apply a <sup>230</sup>Th correction model a value can  
181 be set for the activity ratio and uncertainty of the contaminating material (“A230Th232Th Init.-”). The ~~standard~~  
182 ~~conventional approach value to account for initial Th~~ would be ~~an the bulk earth mean~~ activity ratio of 0.75 ±  
183 0.38, ~~assuming an upper continental crust <sup>232</sup>Th/<sup>238</sup>U weight ratio of 3.8~~ (Taylor and McLennan, 1985) ~~with an~~  
184 ~~uncertainty of 50%~~ (Ludwig and Paces, 2002) ~~and <sup>230</sup>Th, <sup>234</sup>U, and <sup>238</sup>U in secular equilibrium for the detrital~~  
185 ~~material~~. Exemplary templates for corals and speleothems with conventionally used correction models are  
186 provided. For speleothems, a typical activity ratio of (<sup>230</sup>Th/<sup>232</sup>Th)<sub>ini/detr</sub> of detritus is estimated to 0.75 ± 0.38 (~~see~~  
187 ~~above~~), which is derived from a bulk earth Th/U weight ratio of 4.1 ± 2.05 (Wedepohl, 1995) and the assumption  
188 of <sup>230</sup>Th, <sup>234</sup>U, and <sup>238</sup>U being in secular equilibrium (Cheng et al., 2013). Nevertheless, this ratio may require  
189 adjustment according to local conditions. The coral template assumes as default value an activity ratio of 8 ± 4,  
190 which is estimated for corals dwelling in waters of the northeast Atlantic upper thermocline (Wefing et al., 2017).  
191 For one data series, only one correction constant, the (<sup>230</sup>Th/<sup>232</sup>Th) activity ratio of the contamination, can be

192 added to the calculation. Hence, in case several factors need to be explored, the data series requires repeated  
 193 treatment.



194  
 195 **Figure 1.** Input tab: (1) In the top part the data folder is selected (“directory path”), the constants file (“constants”) can be  
 196 loaded (“load”), edited (“edit”), or created (“new”). In addition, it is possible to set an “output path”. Red boxes show the  
 197 “settings” button to enter metadata for saving, as well as the “run” button to start the analysis. Box (2) shows the custom  
 198 constants box as well as the file overview for the selected folder. In box (3), the plots on the top left show the interpolated  
 199 tailing. On the top right, numerical values of U and Th tailing and hydride correction are presented. The calculated ratios are  
 200 shown in the bottom panel.

201 **Figure 1** shows the layout of the GUI ‘Input’ tab. Once the constants are implemented and the input data are  
 202 selected, it is optional to choose an output path to store the analysis output (Box 1). If no path is specified, the  
 203 results will be stored in the raw data folder. When clicking the settings button next to the output path (highlighted  
 204 in red in Box 1), a menu opens in which the following parameters about the sample can be noted: denomination,  
 205 type of archive, lab numbers, geographic origin, and a general description. The first and last laboratory number  
 206 are automatically read out from the raw data. The final output result files will then be saved in a newly created  
 207 folder under the name  $[\text{labnumber}_1\text{-labnumber}_n]$  denomination in the directory chosen before. The metadata  
 208 information transferred through the GUI dialogue window is stored in a .json file in the respective folder. In the  
 209 ‘custom constants’ panel (Box 2), some settings can be selected, for example, if the blank has already been  
 210 subtracted in the mass spectrometric software or not. Next to this panel, an overview over the files read in from  
 211 the folder is shown. After running the evaluation script with the loaded data and adjusted settings (Button “run”,  
 212 highlighted in red in Box 1), the results of tailing and hydride correction, respectively as well as the calculated  
 213 ratios are displayed in the tab (Box 3). In addition, four excel .xlsx output files are created by the software at this  
 214 stage and stored in the directory path folder: Ratios.xlsx, Tailing.xlsx, PrBlank.xlsx and Intensities.xlsx.  
 215 Ratios.xlsx contains all calculated ratios and their errors as also presented in the GUI (Box 3). Tailing.xlsx  
 216 summarizes the U and Th tailing values (in cps/V  $^{238}\text{U}$ ) for each mass. In PrBlank.xlsx, the average values for

217 each mass of the procedural blank measurements before each standard and sample are presented. Intensities.xlsx  
218 contains the full data tables, with the signals in cps or V for each mass over all cycles. Every standard or sample  
219 has its own sheet.

220 The algorithm of the 'Input' tab starts by reading in the '.exp' measurement files for sample and standard  
221 measurements, process blank (=instrumental background) and Uranium and Thorium abundance sensitivity  
222 measurements. The lines for all cycles for all isotopes are imported into a pandas data frame. Firstly, matrices for  
223 tailing, hydride and process blank correction are produced that are later subtracted from the isotopic masses used  
224 for ratio building. The individual steps are carried out as follows:

- 225 • Tailing: Uranium tailing is determined by measuring the off-masses 228.5, 233.5, 236.5, 236.7, 237.05  
226 and 237.5 before a measurement sequence starts. The first half-mass can be changed between 228.5 and  
227 227.5 as we observed a scatter peak around this mass that switched its exact position every few months.  
228 [Thorium t](#)-tailing off-masses are 227.5, 228.5, 229.5, 230.5 and 231.5. For interpolation to full masses,  
229 we use piecewise cubic Hermite interpolating polynomial fits (Kerber et al. 2023). The masses that  
230 undergo <sup>238</sup>U tailing correction are <sup>233</sup>U, <sup>234</sup>U, <sup>235</sup>U, <sup>236</sup>U, <sup>229</sup>Th, <sup>230</sup>Th and <sup>232</sup>Th, while <sup>232</sup>Th correction is  
231 applied to <sup>229</sup>Th and <sup>230</sup>Th.
- 232 • Hydride isobaric interference: Hydride correction is determined by measuring 239 amu for UH<sup>+</sup> and 233  
233 amu for ThH<sup>+</sup> during the abundance sensitivity measurements. The instrumental background (or  
234 memory) is here referred to as process blank. It is measured between all sample and standard  
235 measurements for 70 s. Typical blank levels afterwards are 0.5 cps for <sup>230</sup>Th and 6 cps for <sup>234</sup>U. The  
236 matrices from these three corrections are then used for data reduction of each isotope.
- 237 • Detector setting: Three main different detector layouts are possible and are detected automatically by the  
238 software: 1) all isotopes on cup, 2) <sup>234</sup>U, <sup>230</sup>Th and <sup>229</sup>Th on SEM and 3) <sup>234</sup>U on FC, <sup>230</sup>Th and <sup>229</sup>Th on  
239 SEM. In normal operation, option 2) and 3) are used, depending on the <sup>234</sup>U concentration of the  
240 respective samples. <sup>234</sup>U signals above 2 mV are measured on the center FC which is the case for the  
241 absolute majority of samples.

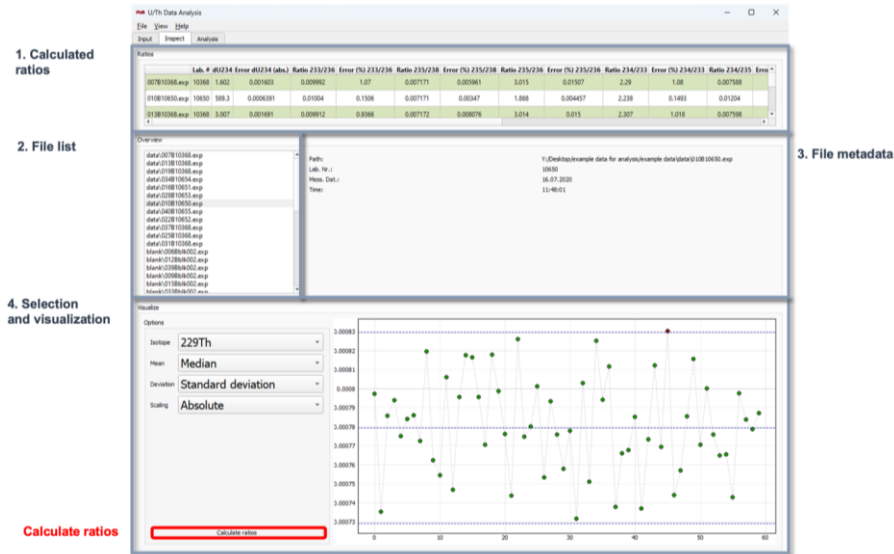
242  
243 of all relevant isotopic ratios followed by subsequent outlier tests, as described in Section 3.2.

### 244 3.2 Inspect Tab

245 Following the initial raw data treatment in the Input Tab, the 'Inspect' tab (presented in [Figure 2](#)) allows to  
246 visualize and retreat the data prior to final age calculation. In particular, the settings for the outlier test can be  
247 adapted.

248 The Inspect tab allows the user to plot the signal datapoints over the measurement cycle number for all isotopes  
249 in the individual measurement files of the sequence. In the top of the tab (1), the ratio results table from the 'Input'  
250 tab is presented. On the left (2), the list of measurement files (.exp) is shown. By clicking on a specific file, the  
251 metadata and the signal plotted over the measurement cycle number are presented (3). On the bottom left (4), four  
252 dropdown menus are available: The first one, "Isotope", allows to select one isotope from all of the isotope species  
253 measured. "Mean" offers to switch between mean and median of the signal. The "Deviation" menu provides three  
254 options for the assessment of data dispersion: standard deviation, median absolute deviation and interquartile

255 range. By setting “Scaling” to absolute or relative, the y-axis of the plot on the right can be changed between  
 256 signal intensities in V or cps and relative values. Any selection in the dropdown menus leads to an automatic  
 257 update of the plot on the right. Mean resp. median, as well as the dispersion ranges are presented as blue dashed  
 258 lines. Data points outside of the dispersion range are marked in red as outliers.



259  
 260 **Figure 2:** Inspect tab. (1) Ratio results table (from Input tab), (2) Overview of measurement files in folder, (3) metadata of a  
 261 selected file and signal over measurement cycle number for one isotope (which can be selected in (4)), (4) option selection  
 262 panel for the signal plotting.



263 The “Calculate ratios” button (5) provides the option to recalculate the ratios using the updated mean and deviation  
 264 selection for all isotopes. The default settings are median and standard deviation. However, these updated options  
 265 are then used to exclude outliers from the ratio arrays, not the signal intensity arrays themselves. This means that  
 266 not necessarily exactly the same data points are marked as outliers in the signal intensity plots and will be  
 267 excluded, but the ones where signal ratios of two isotopes are outside of the accepted deviation range. The option  
 268 selected in “Mean” will then also be used to calculate the average of the isotope ratios.

269 The method of calculating the uncertainty of outlier-corrected isotopic ratios via the standard error, however, is  
 270 fixed. In total, the software provides three different options for dispersion, including (i) the standard deviation (s),  
 271 (ii) the interquartile range (IQR) (Tukey, 1977), and (iii) the median absolute deviation (MAD) (Leys et al., 2013;  
 272 Huber, 2004; Rousseeuw and Croux, 1993).

$$273 \text{err}_{\text{ratio}} = 2 \frac{s}{\sqrt{n}} \quad (1)$$

274 with s being the standard deviation and n the number of data points (after outlier correction). The arithmetic mean  
 275 ( $\bar{x} = \frac{x_1 + \dots + x_n}{n}$ ) and the median  $\bar{M}$  (central value of all values) are different ways of determining the average of a  
 276 distribution. The three different options for dispersion are defined as follows:

277 The standard deviation s is defined as

$$278 s = \sqrt{\frac{1}{n-1} \sum_{i=1}^n (x_i - \bar{x})^2} \quad (2)$$

279 with  $\bar{x}$  being the mean. The interquartile range in turn is defined as the range containing the “middle” 50 % of  
 280 data points (Tukey, 1977). The median absolute deviation MAD is the median of absolute deviations from the  
 281 median, expressed as:

$$282 \text{MAD} = k \cdot M_n(|x_i - \bar{M}|) \quad (3)$$

283 with M being the medians and  $x_i$  the original data (Leys et al., 2013; Huber, 2004; Rousseeuw and Croux, 1993).

284 For the calculation of the uncertainty MAD we assume normal distributed data, thus  $k=1.4286$ . The treatment of  
 285 means of ratios may have undesirable statistical properties for low or fast changing signals (Ogliore et al., 2011;  
 286 Mclean et al., 2016), which could be taken into consideration when updating the software.

### 287 3.3 Analysis tab

288 In a last step, age calculation is carried out in the ‘Analysis’ tab presented in Figure 3. Here, additional input data  
 289 is necessary from the sample weight tables (1). There are several ways to import these tables: Either by clicking  
 290 “Load” and navigating to the respective folder, or by manually creating the table directly in the GUI (“Create”).  
 291 An exemplary weight table is provided in the supplementary data (Figure 1). In the panel “Metadata history”, the  
 292 previously loaded sample weight tables in the directory path folder are shown, and can be directly imported (2).  
 293 “Start Analysis” starts the data analysis and calculates the ages (3). Outputs are both presented in the GUI (4) as  
 294 result table and stored in an Results.xlsx file. In case an output path was specified, Results.xlsx is created both in  
 295 the output and in the directory path folder. If the output path is missing, the file is only saved in the directory path  
 296 folder. If an output directory has been created for specific lab numbers, all following analysis of these same files  
 297 will be written to the same output directory, but not overwrite earlier Results.xlsx. The Results.xlsx has five sheets:  
 298 *Inputs*, *Calc*, *Results*, *Constants* and *Options*. *Inputs* presents sample weight and metadata as well as the calculated  
 299 ratios. In *Calc*, all steps of the age calculation such as concentrations and activity ratios are shown. *Results* is a

Feldfunktion geändert

Formatiert: Standard, Links, Einzug: Links: 0 Pt., Abstand Vor: 0 Pt., Nach: 0 Pt.

Feldfunktion geändert

300 summary of the most important calculation steps and final age values and the same table as is presented in the  
 301 GUI as [\(4\)the results table in figure 3](#). *Constants* contains the whole list of values from the (potentially edited)  
 302 '.cfg' file. In *Options* the average and dispersion measure option are stored.

303 The equations for activity ratios to calculate ages are implemented according to Ivanovich and Harmon (1992),  
 304 with:

$$305 \quad \left(\frac{^{234}\text{U}}{^{238}\text{U}}\right) (t) = \left(\left(\frac{^{234}\text{U}}{^{238}\text{U}}\right)_{init} - 1\right) \cdot e^{-\lambda_{234} \cdot t} + 1 \quad (4)$$

$$306 \quad \left(\frac{^{230}\text{Th}}{^{238}\text{U}}\right) = 1 - e^{-\lambda_{230} t} + \frac{\delta^{234}\text{U}}{1000} \cdot \left(\frac{\lambda_{230}}{\lambda_{230} - \lambda_{234}}\right) \cdot (1 - e^{-(\lambda_{230} - \lambda_{234})t}) \quad (5)$$

307 with

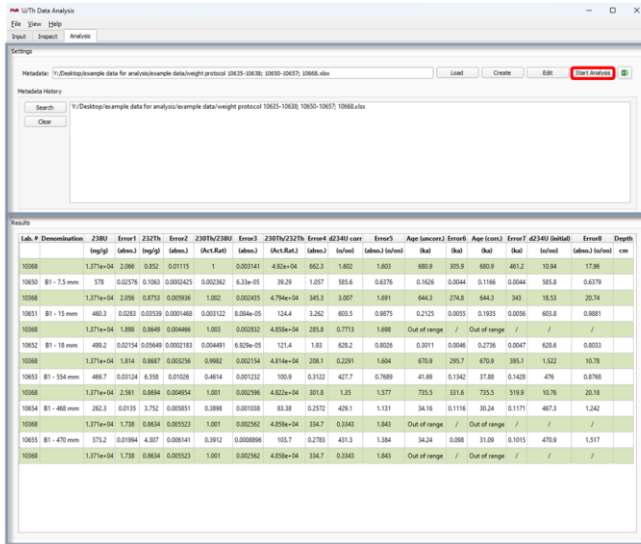
$$308 \quad \delta^{234}\text{U} = \left(\left(\frac{^{234}\text{U}}{^{238}\text{U}}\right)_{meas} - 1\right) \cdot 1000 \text{ (‰)} \quad (6)$$

309 To obtain ages corrected for initial/detrital  $^{230}\text{Th}$ , the  $^{230}\text{Th}/^{238}\text{U}$  activity ratio used in eq. 5 is corrected using the  
 310 initial  $(^{230}\text{Th}/^{232}\text{Th})_{ini/detr}$  ratio and

$$311 \quad \left(\frac{^{230}\text{Th}}{^{238}\text{U}}\right)_{corr} = \left(\frac{^{230}\text{Th}}{^{238}\text{U}}\right)_{meas} - \left(\frac{^{232}\text{Th}}{^{238}\text{U}}\right)_{meas} \cdot \left(\frac{^{230}\text{Th}}{^{232}\text{Th}}\right)_{ini/detr} \cdot \left(\frac{\lambda_{230}}{\lambda_{230} - \lambda_{234}}\right) \cdot e^{-\lambda_{230} \cdot t} \quad (7)$$

312 These equations need to be solved numerically. For the determination of age uncertainty, the usual approach is to  
 313 repeat the numerical determination of the age for several thousand runs in a Monte-Carlo simulation while random  
 314 sampling the input ratios from a normal distribution with  $\mu$  corresponding to the ratio's value and  $\sigma$  corresponding  
 315 to the uncertainty on this parameter.

1. Load metadata  
(weight table)



Start analysis &  
calculate ages

2. Results table

Lab. #	Dimensionisation	ZBR1	Error1	Z327N	Error2	Z397N/Z398I	Error3	Z397N/Z327N	Error4	42340I corr.	Error5	Age (mmort)	Error6	Age (cm)	Error7	42340I (delStat)	Error8	Depth	
		(log/g)	(labm)	(log/g)	(labm)	(kct.Rat)	(labm)	(kct.Rat)	(labm)	(delStat)	(labm)	(delStat)	(delStat)	(delStat)	(delStat)	(delStat)	(delStat)	(delStat)	cm
10360		1.371e-04	2.066	0.852	0.01115	1	0.00141	4.532e-04	662.3	1.602	1.603	680.9	305.9	680.9	461.2	10.94			17.96
10360	B1 - 7.5 mm	578	0.02576	0.1063	0.0002425	0.002362	6.334e-05	39.29	1.057	585.6	0.6376	0.1626	0.0044	0.1166	0.0044	585.8			0.6376
10360		1.371e-04	2.056	0.8753	0.0009396	1.002	0.001405	4.795e-04	345.3	3.007	1.691	644.3	274.8	644.3	341	18.53			20.74
10361	B1 - 15 mm	460.3	0.0283	0.05939	0.0001468	0.003122	8.084e-05	124.4	3.262	605.5	0.8875	0.2125	0.0055	0.1935	0.0056	605.8			0.9881
10360		1.371e-04	1.890	0.8649	0.004466	1.003	0.001832	4.850e-04	285.8	0.7713	1.696	Out of range	/	Out of range	/	/	/	/	/
10360	B1 - 18 mm	499.2	0.02154	0.05649	0.0002183	0.004491	6.929e-05	121.4	1.93	638.2	0.8026	0.3011	0.0046	0.2739	0.0047	638.6			0.8033
10360		1.371e-04	1.814	0.8887	0.002356	0.9962	0.00154	4.814e-04	208.1	0.2291	1.604	670.9	295.7	670.9	395.1	1.522			10.76
10363	B1 - 554 mm	469.7	0.03124	6.558	0.01026	0.4614	0.001232	100.9	0.3122	427.7	0.7889	41.69	0.1342	37.88	0.1428	476			0.8788
10360		1.371e-04	2.561	0.8894	0.004954	1.001	0.002090	4.822e-04	301.8	1.35	1.577	735.3	331.6	735.3	519.9	10.76			20.18
10364	B1 - 468 mm	262.3	0.0185	3.752	0.0008931	0.3898	0.001038	83.38	0.2572	426.1	1.131	34.16	0.1116	30.24	0.1171	487.3			1.242
10360		1.371e-04	1.738	0.8654	0.005523	1.001	0.002562	4.850e-04	334.7	0.3343	1.543	Out of range	/	Out of range	/	/	/	/	/
10365	B1 - 470 mm	373.2	0.01994	4.307	0.008141	0.3912	0.0008966	103.7	0.2783	431.3	1.384	34.24	0.098	31.09	0.1015	470.9			1.517
10360		1.371e-04	1.738	0.8654	0.005523	1.001	0.002562	4.850e-04	334.7	0.3343	1.543	Out of range	/	Out of range	/	/	/	/	/

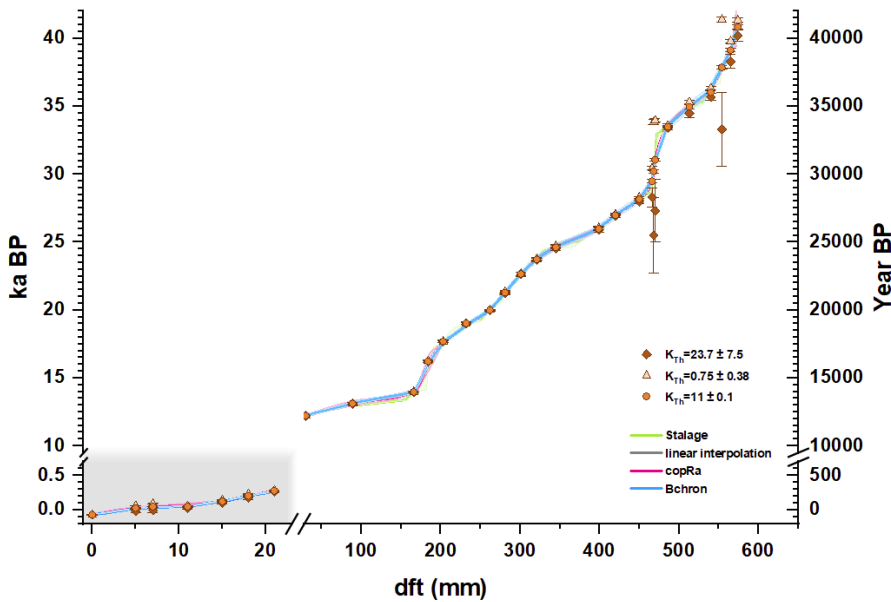
316

317 **Figure 3:** Analysis tab. (1) Load sample weight tables (metadata files). The bottom panel lists the history of previously loaded  
 318 tables. The button highlighted in red starts the analysis to calculate ages ("Start Analysis") button. The panel in box (2)  
 319 displays the results table.

320 **4 Example dataset: Stalagmite B1**

321 To demonstrate our data evaluation tool, we here present newly obtained ages of stalagmite B1 from Larga Cave,  
 322 Puerto Rico. The results of activity ratios and calculated ages can be accessed in the supplementary table S1.  
 323 Analysis of the speleothem samples reveals moderate U concentrations in the range between 300 and 600 ng/g,  
 324 and minor detrital  $^{232}\text{Th}$  contamination with ( $^{230}\text{Th}/^{232}\text{Th}$ ) activity ratios of typically  $>300$ . However, in both the  
 325 top 20 mm and around 450 mm distance from top (dft) lower ( $^{230}\text{Th}/^{232}\text{Th}$ ) activity ratios of c. 40 – 125 are  
 326 measured. U isotopic composition varies between 450 and 640 ‰ of  $\delta^{234}\text{U}$  values. Uncertainties of the uncorrected  
 327 ages are typically in the range of 0.2 to 0.6 % (Table S1). Drip water shows high U concentration of 0.825 ng/g  
 328 and elevated initial Th concentrations, with an activity ratio of  $K=(^{230}\text{Th}/^{232}\text{Th})=11.1 \pm 0.1$ . We have used the  
 329 software to test how the chronology changes to assess the influence of a varying initial Th activity ratio. For this,  
 330 we used three different correction models, including the measured initial Th ratio of the drip water ( $K=11.1 \pm$   
 331  $0.1$ ), the detrital correction value of  $K=0.75 \pm 0.38$  derived from the bulk Earth crust chemical composition, as  
 332 well as a value of  $K=23.7 \pm 7.5$  as previously determined using isochrons on speleothem PR-LA-1 from the same  
 333 cave (Warken et al. 2020).

334 **Figure 4** [Figure S3 in the supplemental material](#) shows the ages corrected for initial  $^{230}\text{Th}$  using the three different  
 335 models. Only the initial  $^{230}\text{Th}$  value measured in the drip water yields a stratigraphic order of the corrected ages  
 336 supporting the use of this value. Residual variability around the mean chronology increases and age inversions  
 337 appear in the record when using a different value of K.

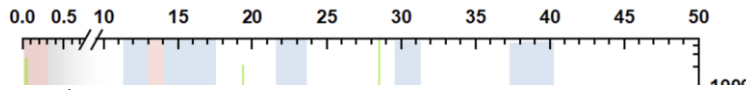


338 **Figure 4:**  $^{230}\text{Th}/\text{U}$  ages and different age-depth simulations for stalagmite B1 using linear interpolation, as well as  
 339 the algorithms Stalage, copRa and behron linear interpolation, as well as the algorithms StalAge (Scholz and  
 340

Formatiert: Block

Formatiert: Standard

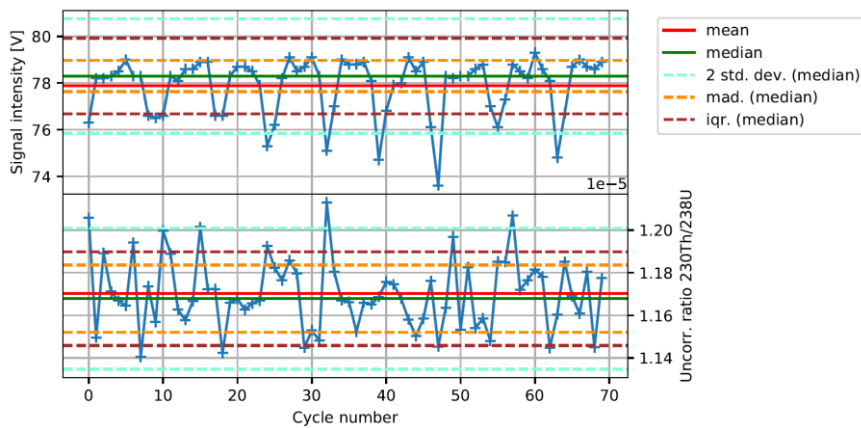
341 Hoffmann, 2011), CopRa (Breitenbach et al., 2012) and Behron (Haslett and Parnell, 2008). Note that the axes  
342 are split at the position of the growth stop at 23 mm dft to visualize the age-depth relationship also during the short  
343 growth phase during the latest Holocene after 0.3 ka BP.



### 345 5.1 Outlier correction

346 Outlier correction is carried out automatically by the software adapting the dispersion measure of the raw data  
347 and in the following we argue that generally means should be replaced by medians. Shao et al. (2019) had  
348 addressed this problem by implementing manual outlier removal by comparison to boxplots based on interquartile  
349 ranges. We opted for the automatic version as this is more time efficient for large datasets. The different dispersion  
350 measure options described in Section 3.2 are relevant because measurements are not always ideal cases with  
351 normally distributed data and thus outliers. During measurements, short-term system instabilities occur for a  
352 variety of reasons, such as varying gas flow in the inlet system, plasma instabilities, and varying size of sample  
353 aerosols causing outliers in the signal intensities. Even though only the ratios between the different isotopes are  
354 of interest, strong changes in signal intensity may lead to varying isotope ratios, as a result of changing variance.  
355 Such difference may be amplified by the use of different detectors or with respect to different magnetic field  
356 settings, which are not necessarily responding at exactly same amplitude. Moreover, signal decreases (detuning  
357 events and temporal clocking) cause the statistical variance to increase locally.

358 [Figure 4](#) shows an example: The upper panel displays periodic dips in the  $^{238}\text{U}$  signal intensity during a  
359 measurement. In the lower panel of Fig. 4, the uncorrected ( $^{230}\text{Th}/^{238}\text{U}$ ) activity ratio for the same measurement is  
360 plotted. For both curves, the different measures to calculate dispersion are shown. ~~The default method (2 standard~~  
361 ~~deviation) does not remove all the systematic outliers. Also,~~ it is clearly visible that the median agrees much  
362 better with the majority of signal intensity values than the mean, which is ~~much~~ ~~strongly~~ ~~er~~ influenced by the  
363 periodic dips due to the asymmetry in the statistical distribution. Such an obvious difference is not visible in the  
364 isotope ratio, but within the resulting uncertainty. Consequently, we propose to generally use the median instead  
365 of mean by default. This is more accurate in the case of asymmetric small-scale oscillations inside the non-outlier  
366 interval and has no disadvantages.



367  
 368 **Figure 446:** Upper panel:  $^{238}\text{U}$  signal intensities in Volt over measurement cycles for a carbonate sample during routine lab  
 369 measurements. Lower panel: Corresponding uncorrected  $^{230}\text{Th}/^{238}\text{U}$  ratio. Mean and median as well as the three different  
 370 dispersion measures are plotted.

371 Applying standard deviation as a dispersion measure in [Figure 4](#)[Figure 4](#)[Figure 6](#) does not cover most of these outliers due to their  
 372 large number and relatively small deviation. Thus, applying another dispersion measure for outlier removal is  
 373 necessary here, and in addition more robust and easier to accomplish than manual deletion of all of the outliers. It  
 374 is important, however, to stress that the outlier correction using the selected dispersion option is run on the  
 375 calculated ratios after correction, not on the signal intensities themselves. This implies that when all isotopes are  
 376 affected in the same way, they pass the outlier test. This is, however, unlikely at least for ratios of isotopes  
 377 measured in different magnetic field settings. The dispersion measure of the outlier corrected ratio array is the  
 378 same in every case, as described [by Equation 1 above](#).

### 379 5.2 Detrital thorium correction

380 Thorium correction is often crucial for studying carbonates where the correction is significant, but the initial  $^{230}\text{Th}$   
 381 value is unknown, -potentially variable, or when studying “dirty” carbonates such as tufa and travertine (Mallick  
 382 and Frank, 2002; Hellstrom, 2006; Wenz et al., 2016). Several studies have shown that this correction [is](#)  
 383 particularly important for speleothem records from the Caribbean and Central American region, where values  
 384 were found including  $2 \pm 1$  (Schorndorf et al., 2023) or  $14 \pm 4$  (Moseley et al., 2015). In Larga Cave, initial  
 385 ( $^{230}\text{Th}/^{232}\text{Th}$ ) ratios are presumably even higher ([Vieten et al., 2024](#); [Warken et al., 2020](#))[where](#) (Warken et al.,  
 386 2020) [obtained a value of  \$23.7 \pm 7.5\$  using isochrons on a stalagmite from the cave](#). Besides the terrestrial regime,  
 387 this aspect is also relevant for marine archive such as corals, where studies propose a large range of seawater  
 388 ( $^{230}\text{Th}/^{232}\text{Th}$ ) activity ratios. While Cheng et al. (2000a) set the range to  $80 \pm 80$  for deep-sea solitary corals, and  
 389 Frank et al. (2004) calculated  $10 \pm 4$  from seawater in the Eastern North Atlantic deep sea, values between 0.4 –  
 390 3.1 were determined for tropical corals (Shen et al., 2008). The range of both absolute values and uncertainties  
 391 for these widely studied archives is hence enormous, and the choice of the appropriate correction model becomes  
 392 particularly important, when (i) samples are very young and have generated only small amounts of  $^{230}\text{Th}$  from U-  
 393 decay, or (ii) when ultra-high precision is at play since any possible correction of the data contribute to the final  
 394 age uncertainty. In our case study, we have run the correction of the ages of stalagmite B1 using three different

395 correction models (Table S1). The resulting differences are visualized in Figure [S34](#), and demonstrate the  
396 significant impact not only on absolute corrected ages, but also their uncertainties. For the young age at 7 mm dft  
397 ( $0.0466 \pm 0.0045$  ka BP), the difference in the absolute corrected age when using another correction factor than the  
398 drip water value of  $K = 11.1 \pm 0.1$  is c.  $\pm 50$  years, which corresponds to a relative difference in the order of 100%  
399 (compare Table S1). Another example is the sample at 554 mm dft ( $37.81 \pm 0.14$  ka BP for  $K = 11.1 \pm 0.1$ ), for which  
400 the other correction models also lead to substantially different ages of  $41.37 \pm 0.19$  ka BP ( $K = 0.75 \pm 0.38$ ) and  
401  $33.3 \pm 2.7$  ka BP ( $K = 23.7 \pm 7.5$ ), hence the differences are still in the range of c. 10%. Notably, the low relative  
402 error of the initial ( $^{230}\text{Th}/^{232}\text{Th}$ ) activity ratio of the drip water results in equally low uncertainties of the corrected  
403 age in the range of 0.4%. In contrast, the relative uncertainty of the age corrected with  $K = 23.7 \pm 7.5$  increases to  
404 8%. Our GUI permits an easy adjustment of the initial ( $^{230}\text{Th}/^{232}\text{Th}$ ) activity ratio for Th correction, which allows  
405 a direct assessment of the resulting corrected ages and uncertainties, and provides thus a convenient basis for  
406 further comparisons of the data. The use of a standardized software instead of handmade tuning reduces the  
407 susceptibility to potential errors, e.g., from copy-pasting, and ensures reproducibility in case a re-evaluation of  
408 the data is required to a later stage.

409 **5.3 In-cave comparison of speleothem growth rates**

410 The high number and precision of  $^{230}\text{Th}/\text{U}$  ages of speleothem B1 allows investigation of growth rates changes.  
411 Comparison with northern hemispheric climatic changes suggests, that speleothem B1 growth is sensitive to  
412 prominent millennial-scale temperature variability, with higher growth rate during warmer phases and vice versa.

413 In particular, during the cooler and drier Heinrich stadials (Warken et al., 2022a), growth rates are reduced.

414 ~~Other differences of the two sites are visible in both speleothems geochemistry, which, however, cannot be directly~~  
415 ~~related to drip rate or cave air  $\text{pCO}_2$  concentration. The Uranium concentration [U] of PR-LA-B1 is systematically~~  
416 ~~higher than for the one of PR-LA-1 (c. 90–400 ng/g) and the initial  $\delta^{234}\text{U}$  is with values ranging between 450 to~~  
417 ~~640 ‰ strongly elevated compared to the  $\delta^{234}\text{U}$  from PR-LA-1, which varies between values of c. 70–100 ‰.~~  
418 ~~This demonstrates a reduced flux of excess  $^{234}\text{U}$  from the host rock at the drip site of PR-LA-1, potentially resulting~~  
419 ~~from varying release of  $^{234}\text{U}$  through alpha-recoil of the decay of  $^{238}\text{U}$  at the two sites. A likely explanation may~~  
420 ~~be the difference in local host rock overburden of PR-LA-B1 with c. 40–60 m to PR-LA-1 with c. 20–40 m, and~~  
421 ~~thus moderately longer residence times of the karst water at site B1. Consequently, given the sum of observations~~  
422 ~~it seems most likely that the GR of PR-LA-1 in the better ventilated region with less rock overburden responds to~~  
423 ~~drip rate more sensitively than PR-LA-B1, which in contrast seems more sensitive to cave ventilation, i.e., cave~~  
424 ~~air  $\text{pCO}_2$ .~~

425 We here provide an algorithm combined with a user-friendly GUI application for [the treatment of  \$^{230}\text{Th}/\text{U}\$  MC-](#)  
426 [ICP-MS data obtained by ThermoFisher Neptune instruments, and subsequent treatment and age calculation and](#)  
427 [correction](#). The two so far published programs explicitly aimed at  $^{230}\text{Th}/\text{U}$  dating data reduction and age  
428 calculation are both written for ThermoFisher Neptune instruments as well. Pourmand et al. (2014) described a  
429 Mathematica routine, distributed as a Computable Document Format (.cdf) file, while Shao et al. (2019) had  
430 published a Matlab algorithm with GUI. We here have chosen to use Python for our algorithm and GUI to keep it  
431 open-source. The advanced user might want to change settings, which makes an opensource language and libraries  
432 a major advantage. However, the stand-alone executable .exe format of the GUI allows user-friendly handling  
433 also for non-programming experts. Our program supports multiple types of detector configurations: the FC-FC  
434 based approach as well as FC-SEM combining protocols. It is however adapted for combined Th and U  
435 measurements in three magnetic field lines (compare Kerber et al. (2023)), but other methods (such as separate  
436 solutions for Th and U) can be implemented with small changes in the code. Furthermore, we offer the first order  
437 Taylor derivation as a time-saving option for uncertainty calculation of final ages. Our application is especially  
438 designed to take reproducible and clear data management into account by a collection of methods: This includes  
439 that automatic creation of folders containing the results files and information on the sample metadata is possible  
440 and that .xlsx output files automatically contain all constants used for calculation, as well as the settings for outlier  
441 correction. Manually changing input constants, e. g. correction, of initial/detrital Th does not require to go to the  
442 code directly. So, the whole analysis scheme does not require any copy-and-pasting from one excel table to the  
443 other, and the constants used for calculation are easy to update.

444 Lastly, we demonstrated our protocols and data analysis scheme by accurately measuring and evaluating 30  
445 speleothem ages from Larga Cave, Puerto Rico. Analyses of the growth rates and comparison with a coevally  
446 growing stalagmite from the same cave highlights the importance of in-cave processes for speleothem deposition  
447 rates.



448 **Author contributions**

449 IK - conceptualized the work, created and tested the implementation and operation of the code, co - supervised  
450 FK, who developed the code for the GUI and tested rigorously all corrections. [AM - has revised and optimized](#)  
451 [the code and made it platform independent](#). NF - conceptualized the project, supervised IK, and FK and quality  
452 controlled the Th U isotope measurements of PR-LA-B1. SW - conceptualized the project, provided guidance on  
453 sample selection, verified the code and conceptualized the application. SW further evaluated the resulting age data  
454 on PR-LA-B1 and supervised a student project during which these and other data had been collected. [All authors](#)  
455 [contributed to the writing and revision of the manuscript](#).

456 **Code availability**

457 The source code of “UTh Data Analysis” is accessible at [https://github.com/EnvArchivesHD/UTh\\_Analysis](https://github.com/EnvArchivesHD/UTh_Analysis).  
458 The folder [https://github.com/EnvArchivesHD/UTh\\_Analysis/tree/main/dist](https://github.com/EnvArchivesHD/UTh_Analysis/tree/main/dist) contains the compiled .exe file for  
459 the GUI (“UTh Data Analysis.exe”) as well as default configuration files (“constants – coral.cfg” and “constants  
460 – stalag.cfg”). The source code of “UTh Analysis” is accessible at [https://github.com/puahd/UTh\\_Analysis](https://github.com/puahd/UTh_Analysis). It is  
461 based on the open source PyQt5 Python library (<https://pypi.org/project/PyQt5/>). To execute the GUI, the user  
462 has to run the file “main.py”. The folder [https://github.com/puahd/UTh\\_Analysis/dist](https://github.com/puahd/UTh_Analysis/dist) also contains a compiled  
463 .exe file for the GUI (“UTh Data Analysis.exe”) as well as default configuration files (“constants – coral.cfg” and  
464 “constants – stalag.cfg”). Example data for the analysis can be found in the supplementary material to this  
465 [publication](#).

Kommentiert [SW1]: Update!!!

466 **Data availability**

467 Results of speleothem B1 <sup>230</sup>Th/U dating are available in the online supplementary material.

468 **Sample availability**

469 Sample material is available on request to [swarken@iup.uni-heidelberg.de](mailto:swarken@iup.uni-heidelberg.de)

Feldfunktion geändert

470 **Competing interests**

471 At least one of the (co-)authors is a member of the editorial board of Geochronology.

472 **Disclaimer**

473

474 **Acknowledgements**

475 The authors are very thankful to the enormous support of the whole team of the research group „Physics of  
476 Environmental Archives” at Heidelberg University. Special thanks go to R. Eichstädter and A. Schröder-Ritzrau

477 for continuous engagement in the laboratory work and quality control. J. Arps is thanked for the development of  
478 a previous version of „UTh-Analysis“. We are particularly grateful to R. Vieten for continuous support of  
479 speleothem research in Larga Cave. R. Vieten, N. Schorndorf, S. Therre and J. Förstel are thanked for their help  
480 in the field and with sample collection. We greatly acknowledge the work of N. Schorndorf, J. Schandl, and J.  
481 Gafriller on, and A. Mielke on the chronology of speleothem B1. J. Bühler, C. Roesch, and K. Rehfeld are thanked  
482 for providing access and support with the age-depth modelling code. N. Frank received financial support for  
483 <sup>230</sup>Th/U measurements (DFG Grant N°256561558) and for the installation of the MC-ICPMS facility (DFG Grant  
484 N°247825108). S. Warken received financial support for the climate study of Puerto Rican speleothems via the  
485 DFG (Grant N° 512385350) and by Heidelberg University via the Olympia Morata program.

#### 486 References

487 Akers, P. D., Brook, G. A., Railsback, L. B., Liang, F. Y., Iannone, G., Webster, J. W., Reeder, P. P.,  
488 Cheng, H., and Edwards, R. L.: An extended and higher-resolution record of climate and land use from  
489 stalagmite MC01 from Macal Chasm, Belize, revealing connections between major dry events, overall  
490 climate variability, and Maya sociopolitical changes, *Palaeogeography Palaeoclimatology*  
491 *Palaeoecology*, 459, 268-288, 10.1016/j.palaeo.2016.07.007, 2016.

492 Akers, P. D., Brook, G. A., Railsback, L. B., Cherkinsky, A., Liang, F., Ebert, C. E., Hoggarth, J. A.,  
493 Awe, J. J., Cheng, H., and Edwards, R. L.: Integrating U-Th, 14C, and 210Pb methods to produce a  
494 chronologically reliable isotope record for the Belize River Valley Maya from a low-uranium  
495 stalagmite, *The Holocene*, 29, 1234-1248, 10.1177/0959683619838047, 2019.

496 Andersen, M. B., Stirling, C. H., Potter, E. K., and Halliday, A. N.: Toward epsilon levels of  
497 measurement precision on 234U/238U by using MC-ICPMS, *International Journal of Mass*  
498 *Spectrometry*, 237, 107-118, 10.1016/j.ijms.2004.07.004, 2004.

499 Beck, J. W., Richards, D. A., Edwards, R. L., Silverman, B. W., Smart, P. L., Donahue, D. J., Herrera-  
500 Osterheld, S., Burr, G. S., Calsoyas, L., Jull, A. J., and Biddulph, D.: Extremely large variations of  
501 atmospheric 14C concentration during the last glacial period, *Science*, 292, 2453-2458,  
502 10.1126/science.1056649, 2001.

503 Bourdon, B., Turner, S., Henderson, G. M., and Lundstrom, C. C.: Introduction to U-series  
504 Geochemistry, *Reviews in Mineralogy and Geochemistry*, 52, 1-21, 10.2113/0520001 %J Reviews in  
505 *Mineralogy and Geochemistry*, 2003.

506 Breton, T., Lloyd, N. S., Trinquier, A., Bouman, C., and Schwieters, J. B.: Improving Precision and  
507 Signal/Noise Ratios for MC-ICP-MS, *Procedia Earth and Planetary Science*, 13, 240-243,  
508 <https://doi.org/10.1016/j.proeps.2015.07.056>, 2015.

Kommentiert [SW2]: Update

Feldfunktion geändert

Formatiert: Englisch (Vereinigte Staaten)

Formatiert: Englisch (Vereinigte Staaten)

509 Cheng, H., Adkins, J., Edwards, R. L., and Boyle, E. A.: U-Th dating of deep-sea corals, *Geochimica*  
510 *et Cosmochimica Acta*, 64, 2401-2416, [https://doi.org/10.1016/S0016-7037\(99\)00422-6](https://doi.org/10.1016/S0016-7037(99)00422-6), 2000a.

511 Cheng, H., Edwards, R. L., Hoff, J., Gallup, C. D., Richards, D. A., and Asmerom, Y.: The half-lives  
512 of uranium-234 and thorium-230, *Chemical Geology*, 169, 17-33, 10.1016/s0009-2541(99)00157-6,  
513 2000b.

514 Cheng, H., Lawrence Edwards, R., Shen, C.-C., Polyak, V. J., Asmerom, Y., Woodhead, J., Hellstrom,  
515 J., Wang, Y., Kong, X., Spötl, C., Wang, X., and Calvin Alexander, E.: Improvements in <sup>230</sup>Th dating,  
516 <sup>230</sup>Th and <sup>234</sup>U half-life values, and U–Th isotopic measurements by multi-collector inductively  
517 coupled plasma mass spectrometry, *Earth and Planetary Science Letters*, 371-372, 82-91,  
518 10.1016/j.epsl.2013.04.006, 2013.

519 Chiang, H.-W., Lu, Y., Wang, X., Lin, K., and Liu, X.: Optimizing MC-ICP-MS with SEM protocols  
520 for determination of U and Th isotope ratios and <sup>230</sup>Th ages in carbonates, *Quaternary Geochronology*,  
521 50, 75-90, 10.1016/j.quageo.2018.10.003, 2019.

522 Douville, E., Sallé, E., Frank, N., Eisele, M., Pons-Branchu, E., and Ayrault, S.: Rapid and accurate U–  
523 Th dating of ancient carbonates using inductively coupled plasma-quadrupole mass spectrometry,  
524 *Chemical Geology*, 272, 1-11, 10.1016/j.chemgeo.2010.01.007, 2010.

525 Dreybrodt, W.: Chemical kinetics, speleothem growth and climate, *Boreas*, 28, 347-356, 1999.

526 Dutton, A., Rubin, K., McLean, N., Bowring, J., Bard, E., Edwards, R. L., Henderson, G. M., Reid, M.  
527 R., Richards, D. A., Sims, K. W. W., Walker, J. D., and Yokoyama, Y.: Data reporting standards for  
528 publication of U-series data for geochronology and timescale assessment in the earth sciences,  
529 *Quaternary Geochronology*, 39, 142-149, <https://doi.org/10.1016/j.quageo.2017.03.001>, 2017.

530 Fensterer, C., Scholz, D., Hoffmann, D., Mangini, A., and Pajón, J. M.: <sup>230</sup>Th/U-dating of a late  
531 Holocene low uranium speleothem from Cuba, *IOP Conference Series: Earth and Environmental*  
532 *Science*, 9, 012015, 10.1088/1755-1315/9/1/012015, 2010.

533 Frank, N., Paterne, M., Ayliffe, L., van Weering, T., Henriot, J.-P., and Blamart, D.: Eastern North  
534 Atlantic deep-sea corals: tracing upper intermediate water  $\Delta^{14}\text{C}$  during the Holocene, *Earth and*  
535 *Planetary Science Letters*, 219, 297-309, 10.1016/s0012-821x(03)00721-0, 2004.

536 Hellstrom, J.: Rapid and accurate U/Th dating using parallel ion-counting multi-collector ICP-MS,  
537 *Journal of Analytical Atomic Spectrometry*, 18, 10.1039/b308781f, 2003.

**Formatiert:** Englisch (Vereinigte Staaten)

**Feldfunktion geändert**

**Formatiert:** Englisch (Vereinigte Staaten)

**Feldfunktion geändert**

**Formatiert:** Englisch (Vereinigte Staaten)

**Formatiert:** Englisch (Vereinigte Staaten)

538 Hellstrom, J.: U–Th dating of speleothems with high initial  $^{230}\text{Th}$  using stratigraphical constraint,  
539 Quaternary Geochronology, 1, 289-295, 2006.

540 Hoffmann, D. L., Prytulak, J., Richards, D. A., Elliott, T., Coath, C. D., Smart, P. L., and Scholz, D.:  
541 Procedures for accurate U and Th isotope measurements by high precision MC-ICPMS, International  
542 Journal of Mass Spectrometry, 264, 97-109, 10.1016/j.ijms.2007.03.020, 2007.

543 Huang, S., Cai, Y., Cheng, H., Xue, G., Cheng, X., He, M., Li, R., Ma, L., Wei, Y., Lu, Y., Yang, L.,  
544 and Edwards, R. L.: An integrated study of constraining the initial  $^{230}\text{Th}$  of a stalagmite and its  
545 implications, Quaternary Geochronology, 80, 101497, <https://doi.org/10.1016/j.quageo.2024.101497>,  
546 2024.

547 Huber, P. J.: Robust statistics, John Wiley & Sons 2004.

548 Ivanovich, M. and Harmon, R.: Uranium series disequilibrium. Applications to environmental  
549 problems. Clarendon, 1992.

550 Kaufmann, G.: Stalagmite growth and palaeo-climate: the numerical perspective, Earth and Planetary  
551 Science Letters, 214, 251-266, 10.1016/S0012-821X(03)00369-8, 2003.

552 Kerber, I. K., Arps, J., Eichstädter, R., Kontor, F., Dornick, C., Schröder-Ritzrau, A., Babu, A., Warken,  
553 S., and Frank, N.: Simultaneous U and Th isotope measurements for U-series dating using MCICPMS,  
554 Nuclear Instruments and Methods in Physics Research Section B: Beam Interactions with Materials and  
555 Atoms, 539, 169-178, <https://doi.org/10.1016/j.nimb.2023.04.003>, 2023.

556 Leys, C., Ley, C., Klein, O., Bernard, P., and Licata, L.: Detecting outliers: Do not use standard  
557 deviation around the mean, use absolute deviation around the median, Journal of Experimental Social  
558 Psychology, 49, 764-766, <https://doi.org/10.1016/j.jesp.2013.03.013>, 2013.

559 Li, T.-Y., Wang, X., Chen, C.-J., Tan, M., and Wu, Y.: Testing the initial  $^{230}\text{Th}/^{232}\text{Th}$  for “Known  
560 Age Carbonate” and its significance for  $^{230}\text{Th}$  dating and paleoclimate research, Quaternary  
561 International, 607, 113-119, 2022.

562 Ludwig, K. and Paces, J.: Uranium-series dating of pedogenic silica and carbonate, Crater Flat, Nevada,  
563 Geochimica et Cosmochimica Acta, 66, 487-506, 2002.

564 Ludwig, K. R. and Titterton, D. M.: Calculation of  $(^{230}\text{Th})/\text{U}$  Isochrons, Ages, and Errors,  
565 Geochimica Et Cosmochimica Acta, 58, 5031-5042, Doi 10.1016/0016-7037(94)90229-1, 1994.

**Formatiert:** Englisch (Vereinigte Staaten)

**Formatiert:** Englisch (Vereinigte Staaten)

**Feldfunktion geändert**

**Feldfunktion geändert**

**Formatiert:** Englisch (Vereinigte Staaten)

**Formatiert:** Englisch (Vereinigte Staaten)

**Formatiert:** Englisch (Vereinigte Staaten)

**Formatiert:** Englisch (Vereinigte Staaten)

**Feldfunktion geändert**

566 Mallick, R. and Frank, N.: A new technique for precise uranium-series dating of travertine micro-  
567 samples, *Geochimica et Cosmochimica Acta*, 66, 4261-4272, [https://doi.org/10.1016-](https://doi.org/10.1016/S0016-7037(02)00999-7)  
568 [7037\(02\)00999-7](https://doi.org/10.1016/S0016-7037(02)00999-7), 2002.

**Formatiert:** Englisch (Vereinigte Staaten)

**Feldfunktion geändert**

**Formatiert:** Englisch (Vereinigte Staaten)

569 Matos, L., Mienis, F., Wienberg, C., Frank, N., Kwiatkowski, C., Groeneveld, J., Thil, F., Abrantes, F.,  
570 Cunha, M. R., and Hebbeln, D.: Interglacial occurrence of cold-water corals off Cape Lookout (NW  
571 Atlantic): First evidence of the Gulf Stream influence, *Deep Sea Research Part I: Oceanographic*  
572 *Research Papers*, 105, 158-170, 10.1016/j.dsr.2015.09.003, 2015.

573 McLean, N. M., Bowring, J. F., and Gehrels, G.: Algorithms and software for U-Pb geochronology by  
574 LA-ICPMS, *Geochemistry, Geophysics, Geosystems*, 17, 2480-2496,  
575 <https://doi.org/10.1002/2015GC006097>, 2016.

**Feldfunktion geändert**

**Formatiert:** Englisch (Vereinigte Staaten)

**Formatiert:** Englisch (Vereinigte Staaten)

576 Merz, N., Hubig, A., Kleinen, T., Therre, S., Kaufmann, G., and Frank, N.: How the climate shapes  
577 stalagmites—A comparative study of model and speleothem at the Sofular Cave, Northern Turkey,  
578 *Frontiers in Earth Science*, 10, 10.3389/feart.2022.969211, 2022.

579 Moseley, G. E., Richards, D. A., Smart, P. L., Standish, C. D., Hoffmann, D. L., ten Hove, H., and  
580 Vinn, O.: Early–middle Holocene relative sea-level oscillation events recorded in a submerged  
581 speleothem from the Yucatán Peninsula, Mexico, *The Holocene*, 25, 1511-1521, 2015.

582 Ogliore, R., Huss, G., and Nagashima, K.: Ratio estimation in SIMS analysis, *Nuclear instruments and*  
583 *methods in physics research section B: beam interactions with materials and atoms*, 269, 1910-1918,  
584 2011.

585 Pourmand, A., Tissot, F. L. H., Arienzo, M., and Sharifi, A.: Introducing a Comprehensive Data  
586 Reduction and Uncertainty Propagation Algorithm for U-Th Geochronometry with Extraction  
587 Chromatography and Isotope Dilution MC-ICP-MS, *Geostandards and Geoanalytical Research*, n/a-  
588 n/a, 10.1111/j.1751-908X.2013.00266.x, 2014.

589 Rivera-Collazo, I., Winter, A., Scholz, D., Mangini, A., Miller, T., Kushnir, Y., and Black, D.: Human  
590 adaptation strategies to abrupt climate change in Puerto Rico ca. 3.5 ka, *The Holocene*, 25, 627-640,  
591 10.1177/0959683614565951, 2015.

592 Rousseeuw, P. J. and Croux, C.: Alternatives to the Median Absolute Deviation, *Journal of the*  
593 *American Statistical Association*, 88, 1273-1283, 10.1080/01621459.1993.10476408, 1993.

594 Roy-Barman, M. and Pons-Branchu, E.: Improved U–Th dating of carbonates with high initial <sup>230</sup>Th  
595 using stratigraphical and coevality constraints, *Quaternary Geochronology*, 32, 29-39,  
596 <https://doi.org/10.1016/j.quageo.2015.12.002>, 2016.

**Formatiert:** Englisch (Vereinigte Staaten)

**Formatiert:** Englisch (Vereinigte Staaten)

**Feldfunktion geändert**

597 Schorndorf, N., Frank, N., Ritter, S. M., Warken, S. F., Scholz, C., Keppler, F., Scholz, D., Weber, M.,  
598 Aviles Olguin, J., and Stinnesbeck, W.: Mid-to late Holocene sea-level rise recorded in Hells Bells  
599  $^{234}\text{U}/^{238}\text{U}$  ratio and geochemical composition, *Scientific Reports*, 13, 10011, 2023.

600 Shao, Q.-F., Li, C.-H., Huang, M.-J., Liao, Z.-B., Arps, J., Huang, C.-Y., Chou, Y.-C., and Kong, X.-  
601 G.: Interactive programs of MC-ICPMS data processing for  $^{230}\text{Th}/\text{U}$  geochronology, *Quaternary*  
602 *Geochronology*, 51, 43-52, 10.1016/j.quageo.2019.01.004, 2019.

603 Shen, C.-C., Lawrence Edwards, R., Cheng, H., Dorale, J. A., Thomas, R. B., Bradley Moran, S.,  
604 Weinstein, S. E., and Edmonds, H. N.: Uranium and thorium isotopic and concentration measurements  
605 by magnetic sector inductively coupled plasma mass spectrometry, *Chemical Geology*, 185, 165-178,  
606 [https://doi.org/10.1016/S0009-2541\(01\)00404-1](https://doi.org/10.1016/S0009-2541(01)00404-1), 2002.

607 Shen, C.-C., Wu, C.-C., Cheng, H., Lawrence Edwards, R., Hsieh, Y.-T., Gallet, S., Chang, C.-C., Li,  
608 T.-Y., Lam, D. D., Kano, A., Hori, M., and Spötl, C.: High-precision and high-resolution carbonate  
609  $^{230}\text{Th}$  dating by MC-ICP-MS with SEM protocols, *Geochimica et Cosmochimica Acta*, 99, 71-86,  
610 10.1016/j.gca.2012.09.018, 2012.

611 Shen, C.-C., Li, K.-S., Sieh, K., Natawidjaja, D., Cheng, H., Wang, X., Edwards, R. L., Lam, D. D.,  
612 Hsieh, Y.-T., Fan, T.-Y., Meltzner, A. J., Taylor, F. W., Quinn, T. M., Chiang, H.-W., and Kilbourne,  
613 K. H.: Variation of initial  $^{230}\text{Th}/^{232}\text{Th}$  and limits of high precision U–Th dating of shallow-water  
614 corals, *Geochimica et Cosmochimica Acta*, 72, 4201-4223, 10.1016/j.gca.2008.06.011, 2008.

615 Skiba, V. and Fohlmeister, J.: Contemporaneously growing speleothems and their value to decipher in-  
616 cave processes—A modelling approach, *Geochimica et Cosmochimica Acta*, 348, 381-396, 2023.

617 Steidle, S. D., Warken, S. F., Schorndorf, N., Förstel, J., Schröder-Ritzrau, A., Moseley, G. E., Spötl,  
618 C., Aviles, J., Stinnesbeck, W., and Frank, N.: Reconstruction of Middle to Late Quaternary sea level  
619 using submerged speleothems from the northeastern Yucatán Peninsula, *Journal of Quaternary Science*,  
620 10.1002/jqs.3365, 2021.

621 Stinnesbeck, W., Rennie, S. R., Avilés Olguín, J., Stinnesbeck, S. R., Gonzalez, S., Frank, N., Warken,  
622 S., Schorndorf, N., Kregel, T., and Velázquez Morlet, A.: New evidence for an early settlement of the  
623 Yucatán Peninsula, Mexico: The Chan Hol 3 woman and her meaning for the Peopling of the Americas,  
624 *Plos one*, 15, e0227984, 2020.

625 Taylor, S. R. and McLennan, S. M.: *The continental crust: its composition and evolution*, 1985.

626 Töchterle, P., Steidle, S. D., Edwards, R. L., Dublyansky, Y., Spötl, C., Li, X., Gunn, J., and Moseley,  
627 G. E.:  $^{230}\text{Th}/\text{U}$  isochron dating of cryogenic cave carbonates, *Geochronology*, 4, 617-627, 2022.

Feldfunktion geändert

Formatiert: Englisch (Vereinigte Staaten)

Formatiert: Englisch (Vereinigte Staaten)

- 628 Tukey, J. W.: Exploratory data analysis, Reading, MA1977.
- 629 Vieten, R. and Hernandez, F.: StalGrowth—A Program to Estimate Speleothem Growth Rates and  
630 Seasonal Growth Variations, *Geosciences*, 11, 187, 2021.
- 631 Vieten, R., Warken, S., Winter, A., Schröder-Ritzrau, A., Scholz, D., and Spötl, C.: Hurricane Impact  
632 on Seepage Water in Larga Cave, Puerto Rico, *Journal of Geophysical Research: Biogeosciences*, 123,  
633 879-888, 10.1002/2017jg004218, 2018a.
- 634 Vieten, R., Winter, A., Warken, S. F., Schröder-Ritzrau, A., Miller, T. E., and Scholz, D.: Seasonal  
635 temperature variations controlling cave ventilation processes in Cueva Larga, Puerto Rico, *International  
636 Journal of Speleology*, 45, 259-273, 10.5038/1827-806x.45.3.1983, 2016.
- 637 Vieten, R., Warken, S., Winter, A., Scholz, D., Miller, T., Spötl, C., and Schröder-Ritzrau, A.:  
638 Monitoring of Cueva Larga, Puerto Rico—A First Step to Decode Speleothem Climate Records, in:  
639 *Karst Groundwater Contamination and Public Health*, edited by: White, W. B., Herman, J. S., Herman,  
640 E. K., and Rutigliano, M., *Advances in Karst Science*, Springer International Publishing, Cham, 319-  
641 331, 10.1007/978-3-319-51070-5\_36, 2018b.
- 642 Vieten, R., Warken, S. F., Zanchettin, D., Winter, A., Scholz, D., Black, D., Koltai, G., and Spötl, C.:  
643 Northeastern Caribbean rainfall variability linked to solar and volcanic forcing, *Paleoceanography and  
644 Paleoclimatology*, 39, e2023PA004720, 2024.
- 645 Warken, S. F., Vieten, R., Winter, A., Spötl, C., Miller, T. E., Jochum, K. P., Schröder-Ritzrau, A.,  
646 Mangini, A., and Scholz, D.: Persistent Link Between Caribbean Precipitation and Atlantic Ocean  
647 Circulation During the Last Glacial Revealed by a Speleothem Record From Puerto Rico,  
648 *Paleoceanography and Paleoclimatology*, 35, 10.1029/2020pa003944, 2020.
- 649 Warken, S. F., Weißbach, T., Kluge, T., Vonhof, H., Scholz, D., Vieten, R., Schmidt, M., Winter, A.,  
650 and Frank, N.: Last glacial millennial-scale hydro-climate and temperature changes in Puerto Rico  
651 constrained by speleothem fluid inclusion  $\delta^{18}O$  and  $\delta^2H$  values, *Clim. Past*, 18, 167-181, 10.5194/cp-  
652 18-167-2022, 2022a.
- 653 Warken, S. F., Kuchalski, L., Schröder-Ritzrau, A., Vieten, R., Schmidt, M., Höpker, S. N., Hartland,  
654 A., Spötl, C., Scholz, D., and Frank, N.: The impact of seasonal and event-based infiltration on transition  
655 metals (Cu, Ni, Co) in tropical cave drip water, *Rapid Communications in Mass Spectrometry*, 36,  
656 e9278, <https://doi.org/10.1002/rcm.9278>, 2022b.

Feldfunktion geändert

Formatiert: Englisch (Vereinigte Staaten)

Formatiert: Englisch (Vereinigte Staaten)

657 Wefing, A.-M., Arps, J., Blaser, P., Wienberg, C., Hebbeln, D., and Frank, N.: High precision U-series  
658 dating of scleractinian cold-water corals using an automated chromatographic U and Th extraction,  
659 Chemical Geology, 475, 140-148, 10.1016/j.chemgeo.2017.10.036, 2017.

660 Wenz, S., Scholz, D., Sürmelihindi, G., Passchier, C. W., Jochum, K. P., and Andreae, M. O.:  $^{230}\text{Th}/\text{U}$ -  
661 dating of carbonate deposits from ancient aqueducts, Quaternary Geochronology, 32, 40-52, 2016.

662 Wortham, B. E., Banner, J. L., James, E. W., Edwards, R. L., and Loewy, S.: Application of cave  
663 monitoring to constrain the value and source of detrital  $^{230}\text{Th}/^{232}\text{Th}$  in speleothem calcite:  
664 Implications for U-series geochronology of speleothems, Palaeogeography, Palaeoclimatology,  
665 Palaeoecology, 596, 110978, <https://doi.org/10.1016/j.palaeo.2022.110978>, 2022.

666 Zhao, J.-x., Yu, K.-f., and Feng, Y.-x.: High-precision  $^{238}\text{U}$ – $^{234}\text{U}$ – $^{230}\text{Th}$  disequilibrium dating of the  
667 recent past: a review, Quaternary Geochronology, 4, 423-433, 10.1016/j.quageo.2009.01.012, 2009.  
668

Feldfunktion geändert

Formatiert: Englisch (Vereinigte Staaten)

Formatiert: Englisch (Vereinigte Staaten)